Journal of Materials Chemistry A

RSC Publishing

COMMUNICATION

View Article Online
View Journal | View Issue

Cite this: *J. Mater. Chem. A*, 2013, **1**, 194

Received 24th September 2012
Accepted 15th October 2012

DOI: 10.1039/c2ta00416j

www.rsc.org/MaterialsA

Oriented single-crystalline nickel sulfide nanorod arrays: "two-in-one" counter electrodes for dye-sensitized solar cells†

Wei Zhao,‡[ab] Tianquan Lin,‡[a] Shengrui Sun,[a] Hui Bi,[a] Ping Chen,[a] Dongyun Wan*[a] and Fuqiang Huang*[ab]

An oriented millerite nickel sulfide (NiS) nanorod array was successfully grown on bare glass substrate. Metallic conductivity and outstanding electrocatalytic activity make it possible to function as a new type of "two-in-one" counter electrode (CE) in dye-sensitized solar cells (DSCs) to replace both the transparent conductive oxide (TCO) and Pt electrocatalyst. When applied in DSCs, an impressive power conversion efficiency of 7.41% was achieved, comparable to that of TCO supported Pt CE (7.55%). The NiS nanoarray film could be a potential candidate to realize a "two-in-one" CE in DSCs, which is highly desirable to reduce the fabrication cost of DSCs while retaining a comparable conversion efficiency.

Dye-sensitized solar cells (DSCs) have attracted great attention during the last two decades due to their simple fabrication process, low-cost raw materials and relatively high power conversion efficiency (PCE).[1–3] The counter electrode (CE), as an indispensable component of DSCs promoting the catalytic reduction of triiodide ions, plays an important role in determining the PCE of DSCs.[4] An effective CE should have excellent electrocatalytic activity and high electrical conductivity. Currently, the noble metal platinum (Pt) electrocatalyst on a transparent conductive oxide (TCO) substrate is commonly employed as a CE in DSCs and has proven high efficiency and long-term stability. However, in view of the high price of TCO substrate and Pt electrocatalyst (60% of the total cost),[5] exploiting TCO-less electrodes and non-Pt electrocatalysts is highly desirable.[6] This has been realized in photoanode preparation by replacing TCO substrate with titanium metal plate or stainless steel substrate.[7,8] Specifically, in construction of CE, developing non-Pt electrocatalysts such as conducting polymers,[9,10] graphene and graphene-based composites,[11–13] and metal in the form of oxides,[14,15] sulfides,[16–18] selenides,[19] carbides,[20] nitrides[21,22] and phosphides[23] has drawn overwhelming interest in recent years. Although comparable performances have been achieved, an electron collector, for example FTO/ITO and/or conductive carbon layer, is still involved.[5] Few studies explored a new type "two-in-one" CE, aiming at substituting both TCO and Pt with a single material of high conductivity and excellent electrocatalytic activity.[24] To date, fabrication of a totally TCO-free and Pt-free CE for high efficiency DSCs still remains a challenge.[25,26]

Nickel sulfide (NiS) undergoes temperature-dependent metal to insulator transition, which displays metallic conductivity with the resistivity as low as 10^{-5} to 10^{-4} Ω cm at room temperature.[27] Meanwhile, NiS also possesses excellent electrocatalytic activity, and a PCE of 6.83% has been achieved for DSCs by using electrodeposited NiS on FTO substrate as a CE.[28] Combining these two characteristics, NiS could function as electron collector and electrocatalyst simultaneously. Considering that one dimensional (1D) nanoarray can provide short diffusion pathway for electron transport and high surface area for electrolyte adsorption, 1D NiS nanoarray film would be an ideal and promising candidate to realize "two-in-one" CE in DSCs with higher efficiency and lower cost.

Herein, we report a facile one-pot hydrothermal approach to directly grow millerite NiS single-crystalline nanorod arrays (NRAs) on bare glass substrate. The obtained NiS NRAs demonstrate a unique two-layer structure with a top nanorod array layer on a bottom compact layer. The nanorod array not only allows high surface area for more electrocatalytic active points, but also possesses single-crystalline nature to facilitate the electron transfer, while the compact layer functions as electron collector. To the best of our knowledge, this is the first time to realize the direct growth of highly oriented single-crystalline NiS NRA on bare glass substrate, and then to straightforwardly serve as a "two-in-one" CE (Scheme 1). When applied in DSCs, an impressive PCE of 7.41% was achieved, comparable to the device with FTO supported Pt CE (7.55%).

[a]*CAS Key Laboratory of Materials for Energy Conversion and State Key Laboratory of High Performance Ceramics and Superfine Microstructure, Shanghai Institute of Ceramics, Chinese Academy of Sciences, Shanghai 200050, P.R. China. E-mail: wandy@mail.sic.ac.cn; huangfq@mail.sic.ac.cn*

[b]*Beijing National Laboratory for Molecular Sciences and State Key Laboratory of Rare Earth Materials Chemistry and Applications, College of Chemistry and Molecular Engineering, Peking University, Beijing 100871, China*

† Electronic supplementary information (ESI) available: A detailed description of the experimental methods and additional experimental results. See DOI: 10.1039/c2ta00416j

‡ Wei Zhao and Tianquan Lin contributed equally to this work.

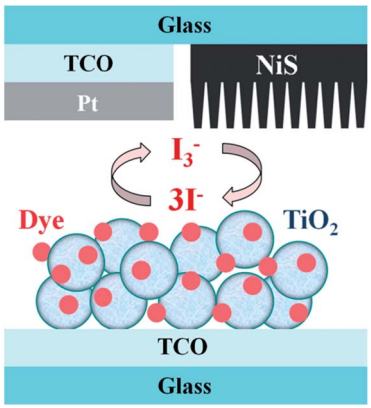

Scheme 1 A typical DSC with a traditional TCO-Pt CE (top-left) and a new type NiS "two-in-one" CE (top-right).

Direct growth of nanostructured thin films on TCO or metal substrates under solvo/hydrothermal conditions has been successfully realized for large quantities of metal oxide,[29] hydroxide[30] or sulfide.[31] In this study, NiS NRAs were hydrothermally deposited on bare glass substrate using low cost raw materials including nickel salt as the nickel source, ammonia as the pH control agent and thiourea as the sulfur source. The samples employed in this study were prepared at 150 °C with different reaction times of 5 h, 10 h, and 20 h, which are correspondingly denoted as G-NiS5, G-NiS10, and G-NiS20. XRD results indicate that the as-deposited film on glass substrate is β-NiS. All the diffraction peaks are indexed to the millerite NiS with lattice constants of $a = 0.962$ nm and $c = 0.3149$ nm (JCPDS no. 12-0041) and no impurity phases are detected (Fig. S1†). Fig. 1a displays the representative SEM top-view image of G-NiS5 sample. It shows that the acquired nanorod has an average diameter of 50 nm (inset in Fig. 1a). The cross-sectional views in Fig. 1b and S2† reveal that the fabricated NRA film has a two-layer structure: a nanorod array layer with 1.29 μm height on a compact layer with 1.57 μm height. With increasing growth time from 10 h to 20 h, the crystallinity of the NRA film is enhanced (Fig. S1†) and the film thickness is increased (Fig. S3†). The adhesion of NRA film on the substrate is strong and it is difficult to scratch the film from the substrate by flowing water and ultrasonication treatment. The nanorod morphology is also confirmed by the TEM image (Fig. 1c). And the lattice fringe spacings of 0.308 nm and 0.286 nm in the HRTEM image (Fig. 1d) correspond to (101) and (300) planes of millerite NiS crystal, respectively, indicating that the nanorods are single-crystalline and have a preferred growth along [001] direction, also as evidenced by the bright SAED pattern of a nanorod examined along the [010] zone axis (inset in Fig. 1d). The chemical stoichiometry of the nanoarray film is examined with EDX and the molar ratio of Ni to S is found to be close to 1 : 1 (Fig. S4†).

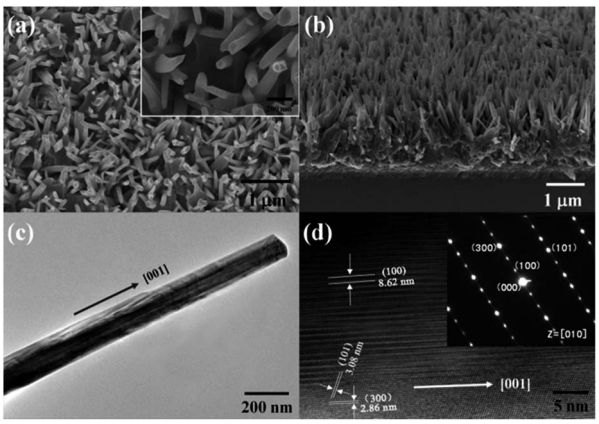

Fig. 1 (a) Top-view SEM image of G-NiS5 (inset: a high magnification SEM image). (b) Cross-sectional SEM view of G-NiS5 with a twist angle of 20°. (c) TEM image of an individual scratched nanorod. (d) HRTEM image of an individual nanorod and inset of the corresponding SAED pattern.

The growth kinetics of such NiS NRAs is investigated by varying the growth conditions. Well aligned rod-like NiS NRA film can only be deposited when the equivalent volume between ammonia and water and the equivalent molar between nickel salt and thiourea are tailored. The two-layer structure of as-deposited NiS NRAs as shown in cross-sectional SEM images (Fig. 1b and S2†) is always obtained. It is proposed that NiS nanoparticles were selectively deposited on the glass surface at the beginning and their aggregation led to the formation of a compact layer, which then served as the seed-layer inducing the growth of top nanorod array layer. A similar growth mechanism has also been proposed for the growth of wurtzite CdS nanorod arrays on ITO substrate due to the similar hexagonal structure of wurtzite CdS and millerite NiS.[32] The direct growth of NRAs from the pre-deposited compact layer would lead to an intimate contact between them and facilitate the electron transfer when applied in optoelectronic devices.

In a typical TCO-supported Pt CE, TCO substrate and noble metal Pt function as electron collector and electrocatalyst for triiodide reduction, respectively. In the present work, NiS NRAs on bare glass substrate are straightforwardly employed as CE in DSCs. As a contrast, FTO-Pt CE is prepared by sputtering Pt with 100 nm thickness on FTO substrate. Because of the insulator nature of bare glass substrate, as a prerequisite being a CE, NiS NRA film on glass substrate must be highly conductive for electron collector and transport. Table 1 lists the sheet resistance (R_{sh}) of NiS NRAs on glass substrate determined by four-point probe technique. It can be seen that all the NiS NRA films have low sheet resistance, significantly less than those of commercial FTO substrate (25 Ω sq^{-1}) and FTO-Pt (5.042 Ω sq^{-1}). Sample G-NiS10 has the lowest value, only 0.3881 Ω sq^{-1}, which can be attributed to a compromise between the crystallinity and the nanorod density. Compared with G-NiS10 and G-NiS20, G-NiS5 has a higher R_{sh} value maybe due to its weaker crystallinity. The R_{sh} value for G-NiS10 is slightly lower to G-NiS20 because of a denser nanorod density (see Fig. S3†). It can provide more nanorods per area for electron transport, leading to a lower R_{sh} value. These low R_{sh} values indicate that all the NiS NRA films exhibit metallic conductivity at room temperature. This characteristic can also be supported by theoretical calculations. Calculated band structure and density of states based on first-principles density functional theory indicate metallic behavior of millerite NiS (more detailed clarification is given after Fig. S5†).[33]

The high conductivity of millerite NiS has been demonstrated by the experimental characterizations and theoretical calculations above. In order to evaluate the electrocatalytic activity of NiS NRA film toward triiodide reduction in an I^-/I_3^- redox solution, cyclic

Table 1 Photovoltaic parameters of DSCs with different counter electrodes and simulated data from fitted EIS spectra

Counter electrode	V_{oc} (V)	J_{sc} (mA cm^{-2})	FF (%)	η (%)	R_s (Ω)	R_{ct} (Ω)	R_{sh} (Ω)
FTO-Pt	0.753	14.54	65	7.55	14	9.06	5.04
G-NiS5	0.722	9.79	62	4.67	5.8	278.4	1.03
G-NiS10	0.765	13.44	68	7.41	3.6	11.73	0.388
G-NiS20	0.734	12.86	63	6.33	2.5	48.16	0.440

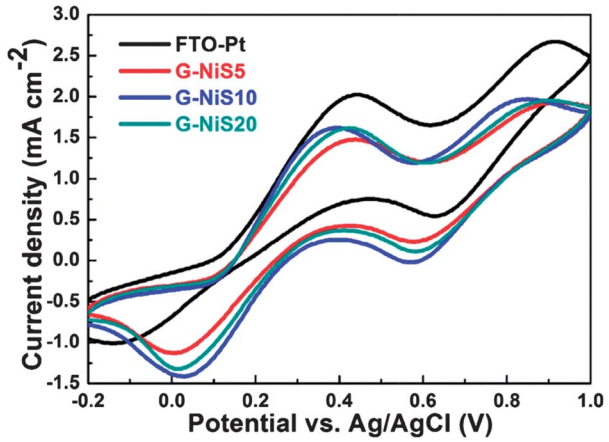

Fig. 2 Cyclic voltammetry for all the three NiS nanoarrays on glass substrate and counterpart FTO-Pt electrode in 10 mM LiI and 1 mM I_2 acetonitrile solution containing 0.1 M $LiClO_4$ as the supporting electrolyte.

voltammetry (CV) measurements are carried out with a FTO-Pt electrode as a reference. As shown in Fig. 2, all the CEs show a typical curve with two pairs of redox peaks and the two cathodic peaks correspond to the two-step process of triiodide reduction. However, NiS NRA film electrodes demonstrate two advantageous features over the FTO-Pt electrode being a CE: (i) cathodic peak potentials are slightly positive than that of FTO-Pt, indicating a lower overpotential for reduction of I_3^- to I^- due to the lower sheet resistance of NiS NRAs. (ii) The cathodic current densities of NiS NRAs are obviously higher than that of FTO-Pt, demonstrating a much faster I^-/I_3^- catalytic rate originating from the more reactive points and faster electron transport in the single-crystalline NiS nanorod. As a result, metallic and highly catalytic NiS NRA film on glass substrate can be a good candidate as "two-in-one" CE for DSCs.

Fig. 3 illustrates the photocurrent density–voltage curves of DSCs with FTO-Pt, G-NiS5, G-NiS10, and G-NiS20 as CEs. The detailed photovoltaic parameters are summarized in Table 1. The DSC with G-NiS10 CE has an open-circuit voltage (V_{oc}) of 0.765 V, a short-circuit current density (J_{sc}) of 12.10 mA cm^{-2}, a fill factor (FF) of 0.68, and a PCE of 7.41%, higher than that of DSCs based on G-NiS5 (4.67%) and G-NiS20 (6.33%) CEs, comparable with FTO-Pt CE (7.55%). This PCE value is also superior to the previous reports on DSCs with electrodeposited Ni_9S_8 CE[28] (6.83% with active area unknown) and solution processed Ni_3S_2 CE[34] (7.01% with an active area of 0.28 cm^2). Such outstanding performance can be attributed to the high surface area NRA with more interfacial active sites for electrolyte anchoring and triiodide reduction, the unique two-layer structure with an intimate contact for effective electron transfer and the oriented single-crystalline NRA with high conductivity for fast electron transport. Direct growth of 1D nanoarray electrodes has been extensively studied in photoanode (TiO_2, ZnO, *etc.*) construction[35–37] and has been demonstrated an encouraging PCE. Similarly, from our study, this strategy is also successfully implemented in the preparation of an effective CE for high efficiency DSCs. Among the as-prepared three NiS CEs, the DSC with G-NiS10 CE displays the best performance, which should be a trade-off between the crystallinity and the surface area. As aforementioned, prolonging the deposition time would lead to the enhanced crystallinity and then improved electron transport and collection capability, however, long time deposition extending to 20 h would result in the thicker NiS rods and reduce the effective active surface area for electrolyte adsorption and triiodide reduction. Either low crystallinity or low surface area would limit the PCE. NiS NRA film was also grown on FTO substrate and PCE for this CE was lower, only 6.2%,

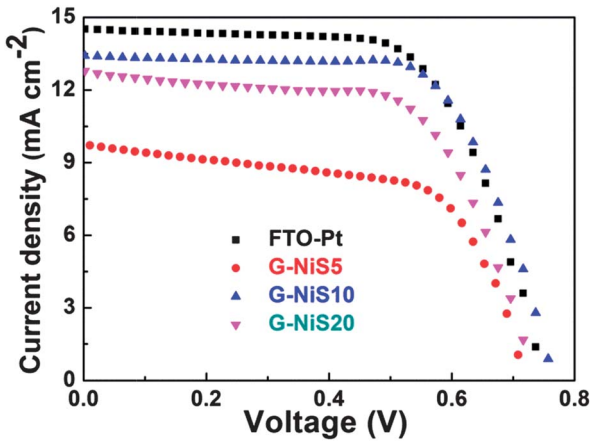

Fig. 3 *J–V* characteristics of DSCs with different CEs measured under simulated sunlight 100 mW cm^{-2} (AM 1.5).

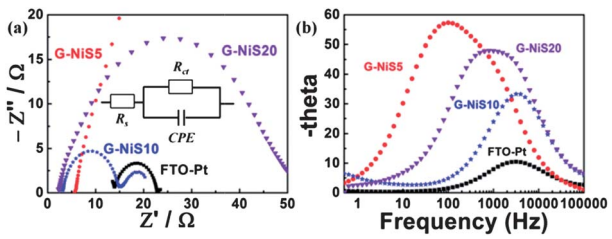

Fig. 4 (a) Nyquist plots of a symmetric cell configuration consisting of two identical NiS, Pt electrodes (inset: a fitted equivalent circuit). (b) Bode plots of four CEs obtained from the EIS spectra.

probably due to the poor adhesion between nanoarray layer and FTO substrate (Fig. S6†). At any rate, it is demonstrated that exploiting an effective "two-in-one" CE for DSCs with a single NiS material is possible. Specifically, the unique two-layer structure plays the vital role: the bottom compact layer fully coating the insulating glass substrate functions as the electron collector for electron transport and the top nanorod layer functions as the catalytic center for electrolyte adsorption and triiodide reduction.

To further study the electron transport process at the CE/electrolyte interface and evaluate the catalytic activity of the CEs, electrochemical impedance spectroscopy (EIS) is measured in a symmetric cell configuration consisting of two identical CEs. Fig. 4a shows the obtained Nyquist plots conducted in the dark with no bias potential, which are fitted with an equivalent circuit (inset in Fig. 4a). The semicircle at the high frequency region presents the charge transfer resistance (R_{ct}) at the CE/electrolyte interface. The ohmic series resistance (R_s) and R_{ct} can be derived in Table 1. Clearly, all the NiS CEs have smaller R_s values compared with FTO-Pt CE, which agrees well with the sheet resistance (R_{sh}) comparison. Generally, FF is inversely proportional to R_s. But, for G-NiS5 and G-NiS20 CEs, the results are anomalous for this relationship. This may be due to their poor charge transfer ability (much higher R_{ct} values compared with FTO-Pt CE) because both R_{ct} and R_s have an impact on FF. Among the three NiS CEs, the G-NiS10 CE possesses the lowest R_{ct} of 11.73 Ω, close to the value of FTO-Pt CE (9.06 Ω), indicating the fastest charge transfer in G-NiS10 electrode. Bode plots shown in Fig. 4b depict the relationship between the phase of the impedance of DSCs and frequency of the input AC voltage. Generally, the peak located at high frequency relates to reactions at CE/electrolyte interface and its intensity falls with the decrease in R_{ct}.[38] Obviously, the G-NiS10 and FTO-Pt CEs have lower peak intensity than that of the G-NiS5 and G-NiS20 CEs, yielding higher efficiency of DSCs owing to the lower R_{ct}. These EIS results completely agree with the CV analysis and the photovoltaic performance of DSCs.

Combining the R_{sh} measurement, electrochemical analysis and photovoltaic performance characterization of our fabricated NiS NRA film, it is proved that constructing an effective "two-in-one" CE for high efficient DSCs with a single material is definitely possible. Inspired by our study, it is necessary to seek other functional materials with high conductivity and outstanding electrocatalytic activity simultaneously, aiming at further reducing the production cost of DSCs.

In summary, millerite NiS single-crystalline NRAs have been successfully deposited on bare glass substrate *via* a facile one-pot hydrothermal method. The as-prepared NiS NRAs show high surface area for electrolyte anchoring, high conductivity and short diffusion pathway for electron transport, and excellent electrocatalytic activity for triiodide reduction. They can be straightforwardly implemented as CEs in DSCs, replacing TCO and Pt simultaneously. The DSC assembled can achieve a maximum light conversion efficiency of 7.41%. It is demonstrated that NiS NRA film can be a potential low-cost candidate to implement highly effective "two-in-one" CEs for DSCs. It is also desirable to explore other similar low-cost functional CE materials to further reduce the manufacture cost of DSCs.

Acknowledgements

Financial supports from National 973 & 863 Program of China Grant no. 2009CB939900 and 2011AA050505, NSF of China Grant no. 51202274, 50821004, 61106088, 50902143, 21101164, 61076062 and 51102263, Science and Technology Commission of Shanghai Grant no. 10JC1415800, National Science and Technology Major Project Grant no. 2011ZX02707.

Notes and references

1 B. O'regan and M. Gratzel, *Nature*, 1991, **353**, 737–740.
2 A. Hagfeldt, G. Boschloo, L. Sun, L. Kloo and H. Pettersson, *Chem. Rev.*, 2010, **110**, 6595–6663.
3 A. Yella, H. W. Lee, H. N. Tsao, C. Yi, A. K. Chandiran, M. K. Nazeeruddin, E. W. G. Diau, C. Y. Yeh, S. M. Zakeeruddin and M. Grätzel, *Science*, 2011, **334**, 629–634.
4 N. Papageorgiou, *Coord. Chem. Rev.*, 2004, **248**, 1421–1446.
5 Y. Wang, M. Wu, X. Lin, Z. Shi, A. Hagfeldt and T. Ma, *J. Mater. Chem.*, 2012, **22**, 4009–4014.
6 M. Wu, X. Lin, Y. Wang, L. Wang, W. Guo, D. Qi, X. Peng, A. Hagfeldt, M. Grätzel and T. Ma, *J. Am. Chem. Soc.*, 2012, **134**(7), 3419–3428.
7 Y. Kashiwa, Y. Yoshida and S. Hayase, *Appl. Phys. Lett.*, 2008, **92**, 033308.
8 H. G. Yun, M. Kim, M. G. Kang and I. H. Lee, *Phys. Chem. Chem. Phys.*, 2012, **14**, 6448–6451.
9 Q. Tai, B. Chen, F. Guo, S. Xu, H. Hu, B. Sebo and X. Z. Zhao, *ACS Nano*, 2011, **5**(5), 3795–3799.
10 R. Trevisan, M. Döbbelin, P. P. Boix, E. M. Barea, R. Tena-Zaera, I. Mora-Seró and J. Bisquert, *Adv. Energy Mater.*, 2011, **5**(1), 781–784.
11 J. D. Roy-Mayhew, D. J. Bozym, C. Punckt and I. A. Aksay, *ACS Nano*, 2010, **4**(10), 6203–6208.
12 L. Kavan, J. H. Yum and M. Grätzel, *ACS Nano*, 2011, **5**(1), 165–172.
13 H. Wang and Y. H. Hu, *Energy Environ. Sci.*, 2012, **5**, 8182–8188.
14 M. Wu, X. Lin, A. Hagfeldt and T. Ma, *Chem. Commun.*, 2011, **47**, 4535–4537.
15 X. Lin, M. Wu, Y. Wang, A. Hagfeldt and T. Ma, *Chem. Commun.*, 2011, **47**, 11489–11491.
16 M. Wang, A. M. Anghel, B. Marsan, N. L. Cevey Ha, N. Pootrakulchote, S. M. Zakeeruddin and M. Grätzel, *J. Am. Chem. Soc.*, 2009, **131**, 15976–15977.
17 M. Wu, Y. Wang, X. Lin, N. Yu, L. Wang, A. Hagfeldt and T. Ma, *Phys. Chem. Chem. Phys.*, 2011, **13**, 19298–19301.
18 H. K. Mulmudi, S. K. Batabyal, M. Rao, R. R. Prabhakar, N. Mathews, Y. M. Lam and S. G. Mhaisalkar, *Phys. Chem. Chem. Phys.*, 2011, **13**, 19307–19309.
19 F. Gong, H. Wang, X. Xu, G. Zhou and Z. S. Wang, *J. Am. Chem. Soc.*, 2012, **134**(26), 10953–10958.
20 M. Wu, X. Lin, A. Hagfeldt and T. Ma, *Angew. Chem., Int. Ed.*, 2011, **50**, 3520–3524.
21 G. Li, F. Wang, Q. Jiang, X. Gao and P. Shen, *Angew. Chem., Int. Ed.*, 2010, **49**, 3653–3656.

22 G. Li, J. Song, G. Pan and X. Gao, *Energy Environ. Sci.*, 2011, **4**, 1680–1683.
23 M. Wu, J. Bai, Y. Wang, A. Wang, X. Lin, L. Wang, Y. Shen, Z. Wang, A. Hagfeldt and T. Ma, *J. Mater. Chem.*, 2012, **22**, 11121–11127.
24 K. S. Lee, H. K. Lee, D. H. Wang, N. G. Park, J. Y. Lee, O. O. Park and J. H. Park, *Chem. Commun.*, 2010, **46**, 4505–4507.
25 K. S. Lee, Y. Lee, J. Y. Lee, J. H. Ahn and J. H. Park, *ChemSusChem*, 2012, **5**, 379–382.
26 B. Lee, D. B. Buchholz and R. Chang, *Energy Environ. Sci.*, 2012, **5**, 6941–6952.
27 S. Krishnakumar, N. Shanthi and D. Sarma, *Phys. Rev. B: Condens. Matter Mater. Phys.*, 2002, **66**, 115101–115106.
28 H. Sun, D. Qin, S. Huang, X. Guo, D. Li, Y. Luo and Q. Meng, *Energy Environ. Sci.*, 2011, **4**, 2630–2637.
29 J. Su, X. Feng, J. D. Sloppy, L. Guo and C. A. Grimes, *Nano Lett.*, 2011, **11**(1), 203–208.
30 J. Li, W. Zhao, F. Huang, A. Manivannan and N. Wu, *Nanoscale*, 2011, **3**, 5103–5109.
31 S. Peng, P. Zhu, V. Thavasi, S. G. Mhaisalkar and S. Ramakrishna, *Nanoscale*, 2011, **3**, 2602–2608.
32 F. Chen, R. Zhou, L. Yang, M. Shi, G. Wu, M. Wang and H. Chen, *J. Phys. Chem. C*, 2008, **112**, 13457–13462.
33 J. H. Wang, Z. Cheng, J. L. Brédas and M. Liu, *J. Chem. Phys.*, 2007, **127**, 214705.
34 H. K. Mulmudi, S. K. Batabyal, M. Rao, R. R. Prabhakar, N. Mathews, Y. M. Lam and S. G. Mhaisalkar, *Phys. Chem. Chem. Phys.*, 2011, **13**, 19307–19309.
35 M. Law, L. E. Greene, J. C. Johnson, R. Saykally and P. Yang, *Nat. Mater.*, 2005, **4**, 455–459.
36 X. Feng, K. Shankar, O. K. Varghese, M. Paulose, T. J. Latempa and C. A. Grimes, *Nano Lett.*, 2008, **8**, 3781–3786.
37 B. Liu and E. S. Aydil, *J. Am. Chem. Soc.*, 2009, **131**, 3985–3990.
38 S. Roy, R. Bajpai, A. K. Jena, P. Kumar, N. Kulshrestha and D. S. Misra, *Energy Environ. Sci.*, 2012, **5**, 7001–7006.

